Bit Patterning in SOAs: Statistical Characterization Through Multicanonical Monte Carlo Simulations

Amirhossein Ghazisaeidi, Francesco Vacondio, Alberto Bononi, *Member, IEEE*, and Leslie Ann Rusch, *Fellow, IEEE*

***Abstract*—We present a simulation tool based on the Multicanonical Monte Carlo (MMC) method to characterize the statistical properties of bit patterning in semiconductor optical amplifiers (SOAs). Our tool estimates the conditional probability density functions (PDFs) of marks and spaces of the received signal. We introduce an experimental technique to directly measure the conditional PDFs of the received marks and spaces using a high bandwidth sampling scope. We demonstrate that predictions from our simulation tool match the experimental data. We measure the bit error rate (BER) of a SOA-based preamplified receiver, where the SOA operates in the nonlinear regime, and demonstrate that our simulation tool can predict the measured BER.**

***Index Terms*—BER, ISI, MMC, modeling, patterning, SOA.**

I. Introduction

ALL-OPTICAL signal processing techniques for future advanced optical networks are now among the key research topics in the optical communication society. The semiconductor optical amplifier (SOA) is instrumental in this context due to its compactness, integrability and rich nonlinear functionality. Some major examples of SOA-based optical signal processing applications include wavelength conversion [1], 2R and 3R all-optical signal regeneration [2], [3], intensity noise suppression [4], inline amplification [5], and this list is by no means exhaustive.

These emerging applications pose new challenges in design and optimization of future optical networks. From the viewpoint of communication systems engineering we need efficient tools to evaluate the performance of optical links via calculation of the bit error rate (BER). A frequently adopted means to evaluate the BER in optical communication is the semi-analytical numerical method based on Karhunen–Loeve (KL) expansion and saddle-point integration [6]. With this technique, the BER can be accurately calculated down to very small values; the lower bound on computable BER is often set by the machine precision. The fiber dispersion, the amplified spontaneous emission (ASE) of linear optical amplifiers, and the Gaussian receiver noise are included, and optical and electrical filters can have arbitrary shapes. The photodetector is modeled as an ideal square-law device in series with a lowpass filter, which can be characterized and absorbed into the electrical filter. However, the major limitation of the KL-based semi-analytical BER calculation technique is the requirement of Gaussian noise statistics before photodetection. Although the Gaussian assumption can be retained in the presence of moderate fiber nonlinearity in special cases [7], the signal-noise interdependency in general limits the applicability of the KL-based method. An example of where the KL-based method is of limited value is the presence of a saturated SOA in the link.

The SOA is a nonlinear element with memory [8]. The nonlinearity of the SOA is mainly due to carrier depletion induced saturation (typical saturation power of SOAs is around 1–10 mW), whereas its memory is due to its finite carrier lifetime (typically about 100–500 ps) [9]. The signal-dependent instantaneous gain of the saturated SOA results in non-Gaussian statistics at the output, and the finite memory of the SOA leads to bit patterning effects, thus resulting in "nonlinear", i.e., signal-dependent enhancement of the intersymbol interference (ISI), on top of the "linear" ISI enhancement stemming from fiber dispersion, optical and electrical filters. The simplest dynamic model for the SOA takes into account saturation and carrier lifetime [10]; while useful in capturing the salient physical mechanisms in SOA operation, this model ignores many other important device characteristics. More realistic SOA models might include distributed carrier-independent loss [11], [12], carrier-dependent loss [12], ASE generated inside the SOA cavity [11]–[13], wavelength dependency of the gain [12], [13], ultrafast dynamics in terms of spectral-hole burning (SHB) and carrier heating (CH) [11], [13], optical Kerr effect [13], group velocity dispersion inside the SOA [13], linewidth enhancement factor dynamics [14], and finally nonlinear polarization rotation [15]. Moreover, the carrier rate equations should be modified if quantum-dot SOAs are investigated. The inclusion of each of these features in the SOA model complicates characterization of the received signal statistics.

Analytical treatments of light statistics at the SOA output are not numerous in the literature, to the authors' knowledge, due to the inherent complexity of the problem. An exact analysis encompassing all the physical mechanisms does not exist. In a recent study, Ohman and Mork apply second-order regular perturbation theory and path integrals to derive analytical expressions for the received signal probability density function (PDF) when the link is composed of a continuous-wave (CW) laser, an SOA, an ideal photodetector, and an arbitrary electrical filter

Manuscript received February 23, 2009; revised July 07, 2009. Current version published February 26, 2010. This work was supported by 2007–2009 Quebec-Italy Executive Program for Scientific Development, Project 13.

A. Ghazisaeidi, F. Vacondio, and L. A. Rusch are with Electrical and Computer Engineering Department, COPL, Université Laval, Quebec, QC, CA (e-mail: amirhossein.ghazisaeidi.1@ulaval.ca; francesco.vacondio.1@ulaval.ca; vacondio@gmail.com; rusch@gel.ulaval.ca; larusch@gmail.com).

A. Bononi is with Dipartimento di Ingegneria dell'Informazione, Universita di Parma, 43100 Parma, Italy (e-mail: bononi@tlc.unipr.it).

Color versions of one or more of the figures in this paper are available online at http://ieeexplore.ieee.org.

Digital Object Identifier 10.1109/JQE.2009.2029545

[16]. The carrier-independent loss and the ASE generated inside the SOA are included, and the SOA operates in saturation. Since the analysis is limited to the CW regime, the resulting expressions are useful for BER prediction only when the nonlinear ISI due to bit-patterning is negligible. In a different approach, Saleh and Habbab [17] consider a typical optical link consisting of an ideal On-Off Keying (OOK) transmitter (TX), emitting square pulses for marks, and zero power for spaces, an SOA, an ideal photodetector and an integrate-and-dump or an RC electrical filter. The SOA model includes only saturation and finite carrier lifetime. By performing simulations on this model they are able to determine the range of bit-rates and power levels where SOA-induced nonlinear ISI enhancement is considerable; however, the only noise source considered in their model for BER evaluation is the Gaussian receiver noise.

Another approach to predicting SOA noise statistics is using computer simulations. Due to the computational complexity of SOA dynamic models, conventional Monte Carlo simulations are of limited value. Bilenca and Eisenstein used Multicanonical Monte Carlo (MMC) to study the PDF of the peak power of a single pulse amplified by the SOA [18], [19]. Their model included ASE generated inside the SOA, and the input pulses where assumed noiseless. In [20] we applied MMC to study intensity noise suppression of spectrum-sliced wavelength division multiplexed (SS-WDM) systems by an SOA. We also described a simple pattern-warping method to improve MMC to jointly warp the bit pattern and the continuous noise sources. Another implementation of pattern-warping within the MMC framework is introduced in [21]. However, in [20] the dominant source of error was noise redistribution of the thermal light source both after the noise-cleaning SOA and after the channel selecting filter, not the small residual linear ISI from optical and electrical filters.

In this paper, which is the extended version of [22], we describe in detail how our simulation tool can be used in practice to predict the BER of optical links including nonlinear SOAs, where ISI is a significant source of error, and provide an experimental validation. The structure of the paper is as follows. In Section II we review the existing theory of the SOA bit patterning. In Section III we introduce our simulation tool. In Section IV we present our experimental technique to probe the memory depth of the SOA, and show that both conditional PDFs of marks and spaces, directly measured in the lab, and the BER can be accurately predicted by our simulation tool. In Section V we conclude.

II. SOA Modeling

In this section we discuss modeling the SOA dynamics and study its impact on bit patterning. The typical link under study is shown in Fig. 1(a), where b_i are the information bits, E_{in} and E_{out} are the optical fields at the SOA input and output respectively, $P_{out} = |E_{out}(t)|^2$ is the detected optical power, and $r(t)$ is the received signal. Our ultimate goal is to study the PDF of $r(t)$ sampled at the decision instant, taking into account the memory and nonlinearity of the channel represented in Fig. 1(a), and to do so, we need to model SOA dynamics.

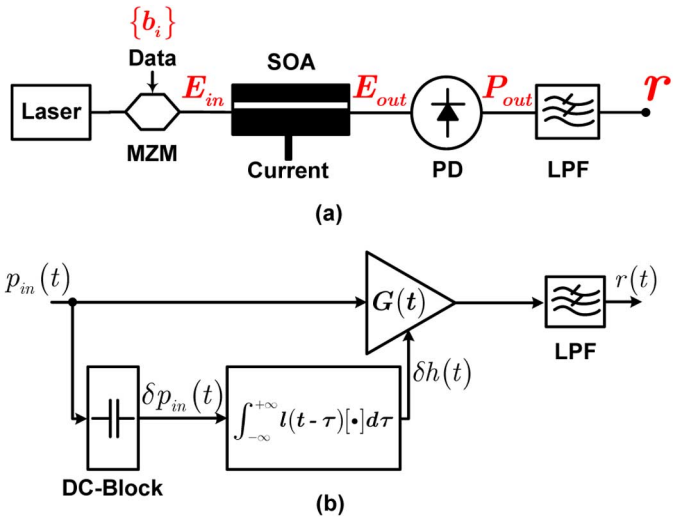

Fig. 1. (a) Basic setup, and)b) block-diagram of the equivalent lowpass SOA model.

The departure point of our study of SOA dynamics is the model presented in [10], which expresses the SOA input and output optical fields through following relations which neglect internal losses:

$$E_{out}(t) = E_{in}(t)e^{\frac{1}{2}(1-j\alpha)h(t)} \tag{1}$$

$$\tau_c \frac{dh(t)}{dt} = h_0 - h(t) - \left(e^{h(t)} - 1\right)\frac{|E_{in}(t)|^2}{P_{sat}} \tag{2}$$

where α is the linewidth enhancement factor, and $h(t)$ is the total integrated gain, τ_c is the carrier lifetime, h_0 is the small-signal total integrated gain, and P_{sat} is the saturation power.

Starting from (1) and (2), the analysis can be conducted in two disparate directions: we can further simplify the model presented in (1) and (2) by applying first-order perturbation, hence deriving small-signal approximations for the received signal [17], [23]–[25]; on the other hand, we can use (1) and (2) to build more elaborate models and study the dynamics numerically [11]. The small-signal model provides insight on the bit patterning mechanism whereas the numerical method provides accuracy. We discuss these two methods in the following subsections.

A. Small-Signal Analytical Model

In the small-signal model, the total integrated gain is written as $h(t) = \bar{h} + \delta h(t)$, where $\bar{h}$ is the average total integrated gain, and $\delta h(t)$ is the zero-mean fluctuations. The input optical power is $P_{in}(t) \triangleq |E_{in}(t)|^2 = \bar{P}_{in} + \delta P_{in}(t)$, where $\bar{P}_{in}$ is the average input power, and δP_{in} is the zero-mean input power fluctuations. Similar definitions hold for the output optical powers: $P_{out}(t) \triangleq |E_{out}(t)|^2 = \bar{P}_{out} + \delta P_{out}(t)$. Furthermore, we normalize all powers to P_{sat}: $p_{in}(t) \triangleq P_{in}(t)/P_{sat}$, $\bar{p}_{in} \triangleq \bar{P}_{in}/P_{sat}$, $\delta p_{in}(t) \triangleq \delta P_{in}(t)/P_{sat}$, with similar definitions for the normalized output powers. The following model for the SOA operation results

$$p_{out}(t) = G(t)p_{in}(t) \tag{3}$$

where

$$G(t) \simeq \bar{G}\,(1+\delta h(t))\,. \tag{4}$$

In (4) we have $\bar{G} \triangleq e^{\bar{h}}$; and $\bar{h}$ satisfies

$$\frac{h_0-\bar{h}}{e^{\bar{h}}-1} = \bar{p}_{in} \tag{5}$$

and

$$\delta h(t) = l(t) \otimes \delta p_{in}(t). \tag{6}$$

In (6) $\otimes$ denotes convolution in time and $l(t)$ is

$$l(t) \triangleq K e^{-t/\tau_{eff}}\, u(t) \tag{7}$$

In (7) $u(t)$ is the unit step function, and K and τ_{eff} are given by the following equations:

$$K \triangleq \frac{1-e^{\bar{h}}}{\tau_c} \tag{8}$$

$$\tau_{eff} \triangleq \frac{\tau_c}{1+\bar{p}_{out}} \tag{9}$$

The equivalent block-diagram of the first-order model is shown in Fig. 1(b). The nonlinearity of the SOA is due to signal-dependent gain, and the memory is due to the impulse response $l(.)$. The input optical power to the SOA is assumed to be an OOK signal:

$$p_{in}(t) = 2\bar{p}_{in} \sum_{n=-\infty}^{\infty} b_n p(t-nT_b) \tag{10}$$

where $b_n \in \{0,1\}$ are the information bits, and $p(\cdot)$ is the ideal rectangular pulse: $p(t) = 1$ for $0 \leqslant t \leqslant T_b$ and $p(t) = 0$ otherwise, and T_b is the bit duration. Substituting (10) into (3), and using (4), (6), and (7) we obtain

$$p_{out}(T_b) = \begin{cases} 2\bar{p}_{out}(1+2\tau_{eff}K\bar{p}_{in}) \\ \quad +4\tau_{eff}K\bar{p}_{in}\bar{p}_{out}z & b_0 = 1 \\ 0 & b_0 = 0 \end{cases} \tag{11}$$

where we have assumed bit b_0 starts at $t = 0$. In (11) z is given by

$$z \triangleq (1-\beta)\sum_{j=0}^{\infty} \bar{b}_{-(j+1)}\beta^j \tag{12}$$

where

$$\beta \triangleq e^{-T_b/\tau_{eff}} \tag{13}$$

and $\bar{b}_i \triangleq 1 - b_i$.

The quantity z is a random geometric series [17], [26], whose exact distribution for arbitrary β is not known. The bit patterning effect resulting from all the preceding bits is captured in z; if all the preceding bits are zero $z = 1$, and if all are one, $z = 0$. For $\beta > 0.5$, Saleh and Habbab [17] use numerical simulations to show z has approximately the following beta distribution:

$$p_Z(z) \cong \frac{\Gamma(2\nu)}{\Gamma^2(\nu)}\,[z(1-z)]^{\nu-1} \tag{14}$$

where $\nu \triangleq \beta/(1-\beta)$.

This small-signal analysis provides a tangible explanation of the bit patterning in SOA; we can isolate in a single random variable z the ISI contribution. Nonetheless, analysis of this random variable is problematic. Furthermore, this analysis lacks precision, since 1) large signal behavior is not included, and 2) many important phenomena, notably the ASE and the distributed loss, are excluded. For these reasons, we turn our attention to more accurate numerical models, as is described in the next subsection.

B. Large Signal Numerical Model

As a fair compromise between computational complexity and completeness, we use the model presented in [11] to model the SOA. As represented in Fig. 2, in this model the SOA cavity is divided into N sections. The instantaneous gain of the i^{th} section is denoted by $G_i(t)$, and we have $G_i(t) \triangleq \exp[h_i(t)]$. The input (output) optical field to the j^{th} section is denoted by $E_{j,I}(t)$ $(E_{j,O}(t))$. The input field to the first section is written as

$$E_{1,I}(t) = E_{in}(t) + \tilde{n}_{ASE}^{SOA}(t) \tag{15}$$

where $E_{in}(t)$ is the optical field input to the SOA, and $\tilde{n}_{ASE}^{SOA}(t)$ models the SOA ASE, as described in [11]. the ASE term is a complex Gaussian noise, white over the simulation bandwidth; the variance of this term is treated as a fitting parameter to match the measured PDFs in Section IV. The input-output optical fields of other sections are related per

$$E_{j,I}(t) = LE_{j-1,O}(t) \quad j = 2,\ldots,N \tag{16}$$

where L is a lumped loss modeling the distributed loss of each section, and is given by

$$L \triangleq \exp\left[-\alpha_{\text{int}}D/(2N)\right] \tag{17}$$

where α_{int} is the SOA distributed loss coefficient, and D is the SOA length. The SOA output field $E_{out}(t)$ is

$$E_{out}(t) = LE_{N-1,O}(t) \tag{18}$$

and the total integrated gain of the j^{th} section

$$\tau_c\frac{dh_j(t)}{dt} = h_0 - h_j(t) - \left(e^{h_j(t)}-1\right)\frac{|E_{j,I}(t)|^2}{P_{sat}} \quad j=1,\ldots,N \tag{19}$$

A unique feature of the model presented in [11] is that (19) can be extended to include SHB and CH if necessary; however, since in this work we will examine NRZ signals at 10 Gb/s, we could safely neglect the ultrafast effects. As per [11], the extension to the ultrafast regime is achieved by complementing (19) with two coupled differential equations for integrated gains due to SHB and CH. This roughly amounts to a three-time increase in computation time. Moreover, while in the ultrafast regime the simulations step time decreases, the bit duration also decreases, so the overhead due to increasing the number of waveform temporal samples results in a fractional increase of computation

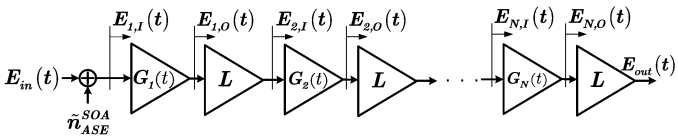

Fig. 2. Large signal SOA model.

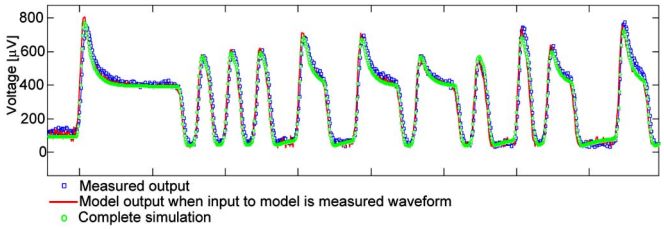

Fig. 3. Measured and simulated SOA waveforms; blue trace is the measured SOA output, red waveform is the SOA model output using measured TX output as input, green waveform is simulation (both TX and SOA).

TABLE I
SOA PARAMETERS USED IN SIMULATIONS

Carrier lifetime, τ_c	170 ps
Saturation power, P_{sat}	13 dBm
small signal total integrated gain, h_0	6.3
Carrier independent loss coefficient, α_{int}	2180 $1/m$
SOA length, D	650 μm
$\hbar\omega_0$	1.28e-19 J

time. The implications of the ultrafast dynamics on the pulse statistics will be addressed in future work.

Fig. 3 illustrates the measured and simulated optical intensities at the SOA output, using 10 sections. The parameters of the SOA that we used in the experiments are given in Table I. As mentioned in the introduction, the nonlinearity of the SOA is mainly due to carrier depletion induced saturation, whereas its memory is due to its finite carrier lifetime. To highlight these dependencies, we vary saturation level and the speed of the SOA response (carrier lifetime) as referenced to the bit rate, as presented in Fig. 4. The eyediagrams are computed using the SOA numerical method described in this subsection. The TX and RX models used in Fig. 4 are described later. Such results numerically support the general trends predicted in the previous subsection. In particular, when the SOA carrier lifetime and the bit duration widely mismatch, i.e., $\beta \to 0$ corresponding to very low bit rate, and $\beta \to 1$ for very high bit rates, the patterning effect vanishes. This trend is predicted by (11) and (12). On the other hand, at any bit-rate, if the SOA is driven more into saturation the term multiplying z in (11) increases, and patterning effect is enhanced.

To summarize, bit patterning is only important when two situations occur. The SOA must be in saturation, e.g., as a booster amplifier, following in-line amplification in 2R or in 3R regenerators. Also, the bit-rate must be comparable with the effective carrier lifetime: when the bit-rate is extremely high [27], or when the carrier lifetimes are very low (for example, novel quantum dot SOAs with high saturation power [28]), the patterning effect becomes less important. In the case of typical commercially available SOAs, and at bit-rates up to 40 Gb/s some residual patterning effect will exist in SOA-based 2R regenerators [3].

III. THE SIMULATOR

Having described the SOA model to be exploited, we now describe the model of the system where the SOA is to be tested (Section III-A). Following that, we describe in Section III-B the MMC simulator that allows us to test system performance down to very low bit error rates with realistic, accurate SOA models.

A. Link Model

1) TX Model: Fig. 5(a) illustrates the lab setup of the transmitter, and Fig. 5(b) shows its numerical model. Logical bits enter the TX subsystem and produce a realistic modulated optical field. $A_{in}(t)$ and $A_{1,out}(t)$ are respectively the optical fields at the output of the laser, and Mach–Zehnder modulator (MZM), and $V(t)$ is the RF data driving the MZM. Note that $A_{in}(t) = \sqrt{\bar{P}_{in}}$ where $\bar{P}_{in}$ will be treated as a fitting parameter including both the laser power and the MZM loss. A lowpass fourth-order Bessel-Thompson (BT4) filter, $H_{TX}(f)$, in Fig. 5(b) smooths the logical bits. This filter is used for its small overshoot, and as it gives good fit with the measured traces; the bandwidth of $H_{TX}(f)$ is set by trial and error, and we normalize to have $H_{TX}(0) = 1$. We use the well-known two-port model of the MZM [30]

$$\begin{bmatrix} A_{1,out}(t) \\ A_{2,out}(t) \end{bmatrix} = \mathbf{Z}(\alpha_1, \alpha_2, V(t), V_b) \begin{bmatrix} A_{in}(t) \\ 0 \end{bmatrix} \tag{20}$$

where

$$\begin{aligned} \mathbf{Z}(\alpha_1, \alpha_2, V(t), V_b) \triangleq & \begin{bmatrix} \sqrt{\alpha_1} & j\sqrt{1-\alpha_1} \\ j\sqrt{1-\alpha_1} & \sqrt{\alpha_1} \end{bmatrix} \\ & \times \begin{bmatrix} e^{j(V(t)-V_b)/2} & 0 \\ 0 & e^{-j(V(t)-V_b)/2} \end{bmatrix} \\ & \times \begin{bmatrix} \sqrt{\alpha_2} & j\sqrt{1-\alpha_2} \\ j\sqrt{1-\alpha_2} & \sqrt{\alpha_2} \end{bmatrix} \end{aligned} \tag{21}$$

and α_1 and α_2 are the power split ratios of the MZM couplers, and V_b is the bias voltage. All voltages in (20) are normalized to V_π/π, where V_π is the voltage inducing a π phase shift in the MZM.

Fig. 6 shows the measured waveform at the output of the transmitter and the simulated result. To achieve this correspondence between experiment and numerical simulation we needed to extract several parameters. For electrical filter BT4, we set the 3 dB bandwidth to $0.8R_b$ where R_b is the bit rate, and then exhaustively searched the 4-dimensional parameter space of all $(\alpha_1, \alpha_2, V_b, \bar{P}_{in})$. We adopted the parameter set where the Euclidean distance between simulated and measured waveforms of a pre-specified sequence is minimum.

The measurements were taken by a high bandwidth sampling scope, the mean noise of which was characterized, and the averaging option was enabled to suppress errors from scope noise.

2) RX Model: Two receivers were employed (cf. Fig. 9): RX1 to measure the conditional PDFs and RX2 to measure the BER. RX1 was an Agilent high bandwidth sampling scope, and RX2 a

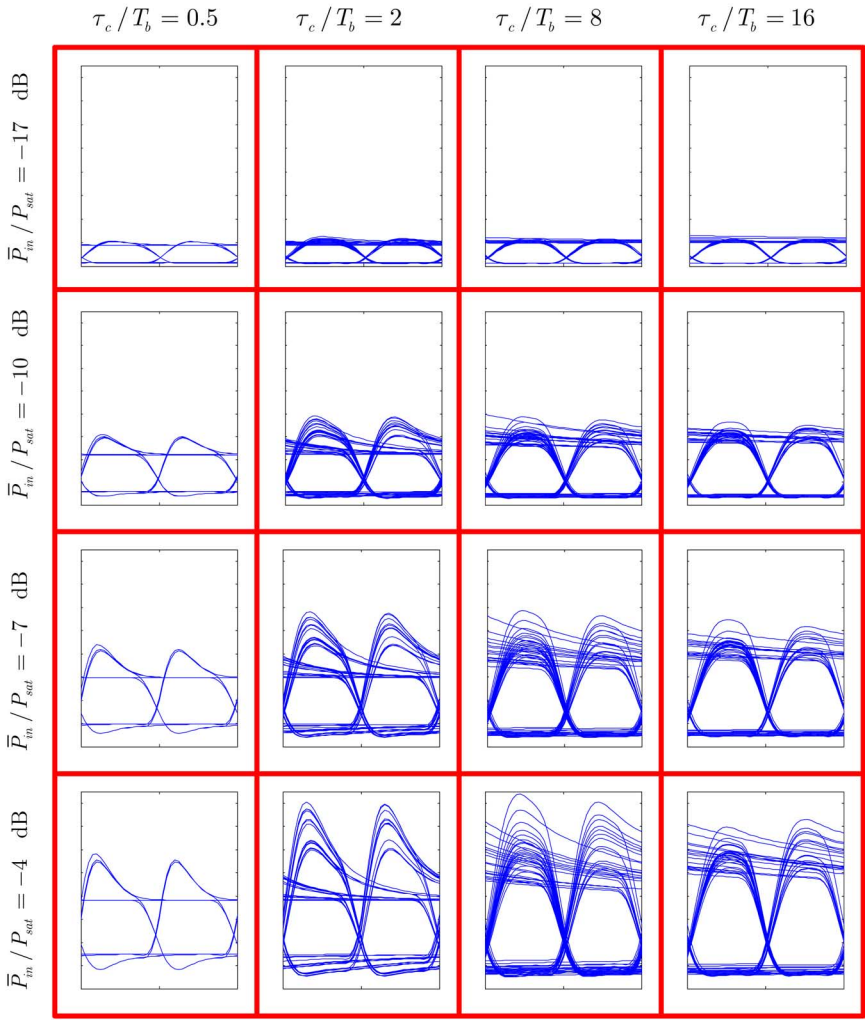

Fig. 4. Eye diagrams at the SOA output for various operational conditions. Bit-rate increases from left to right, and average input power increases from top to bottom.

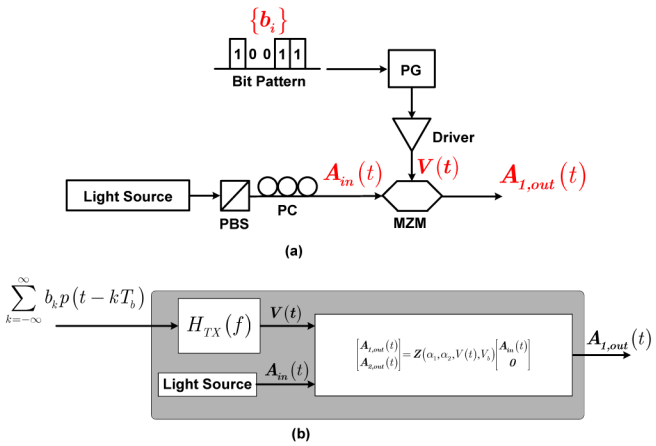

Fig. 5. (a) Transmitter (TX) configuration, (b) TX numerical model; PBS: polarization beam splitter, PC: polarization controller, MZM: Mach–Zehnder modulator.

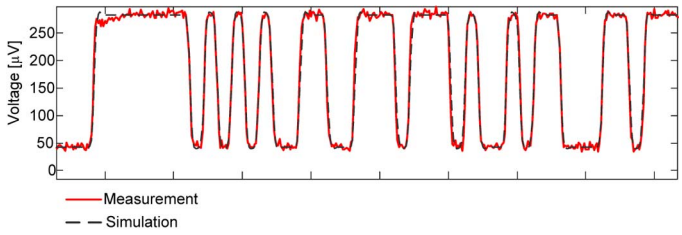

Fig. 6. Optical intensities at the output of the transmitter, measured (blue) and simulated (red).

bit error rate tester. Block diagrams of these receivers are given in Fig. 7(a).

In the case of RX1, we assume the receiver is an ideal square-law device. The receiver noise is denoted by n_R; all the coupling losses either from VOAs or from optical or RF couplings are lumped into G_R. In the case of RX2, G_R contains the RF amplifier gain and all the losses. A white complex Gaussian process, $\tilde{n}_{ASE}^{Rec}(t)$, models the noise generated by the receiver EDFA. In Fig. 7(b) the measured frequency responses of the optical filter $H_{OF}(f)$, the electrical filter $H_{EF}(f)$, and the Agilent photoreceiver $H_{PD}(f)$ are shown.

B. MMC Platform

Referring to Fig. 1, the received signal is

$$r(t) = b_e(t) \otimes P_{out}(t) \tag{22}$$

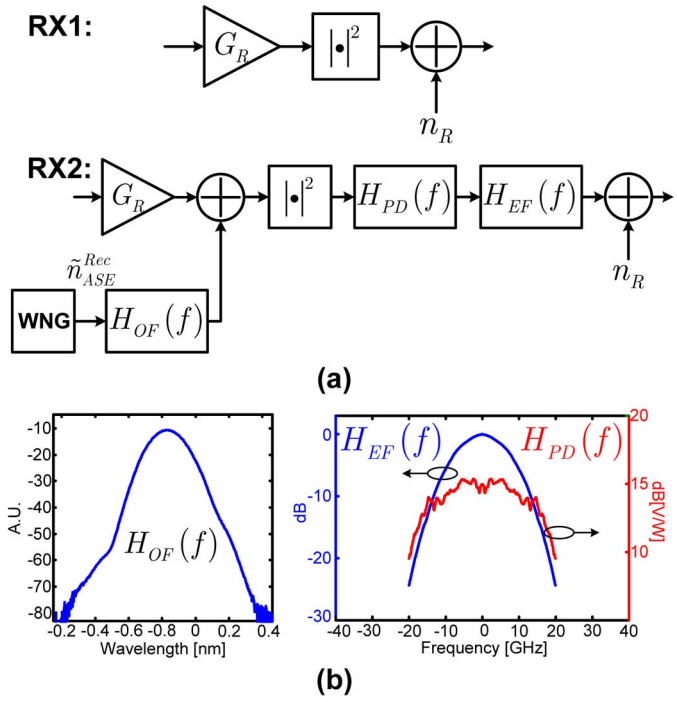

Fig. 7. (a) Numerical models of receivers used in measurements; WNG: white noise generator; (b) frequency domain characterization of RX2.

where $b_e(t)$ is the impulse response of the electrical lowpass filter. The sampled received signal, corresponding to the current bit b_0 is $r_0 \triangleq r(t_s)$, where t_s is the optimum sampling time between 0 and T_b. The conditional PDFs of marks and spaces are written as

$$P_i(r_0) \triangleq p_{r_0|b_0}(r_0|b_0 = i) \tag{23}$$

where $i = 0$ ($i = 1$) corresponds to the conditional PDF of spaces (marks). Assuming that the "effective" memory of the link is M bits, the truncated conditional PDF of marks and spaces is

$$P_{i,M}(r_0) = \frac{1}{2^M} \sum_{\{b_{-1},\ldots,b_{-M}\}} p_{r_0|b_0}(r_0|b_0 = i, b_{-1}, \ldots, b_{-M}) \tag{24}$$

where summation is over all possible patterns of the past M bits. By effective memory we mean $\|P_{i,M}(r_0) - P_{i,M+1}(r_0)\|$ to be sufficiently small for some metric $\|\cdot\|$. We propose to use Multicanonical Monte Carlo method to estimate the effective memory length, and the conditional PDF $P_{i,M}(r_0)$. To determine memory length, we gradually increase M until successively estimated conditional PDFs coincide.

The block-diagram of our MMC simulator is shown in Fig. 8. The numerical system model is composed of three parts (TX, SOA, and RX), all described previously. The details of our MMC platform are presented in [20]. Here we briefly review them.

We denote the simulation time step by Δt, and the number of time samples per bit by N_s, i.e., $T_b = N_s \Delta t$. Assuming the effective memory is M, the past MN_s time samples of all independent noise sources have an impact on the distribution of

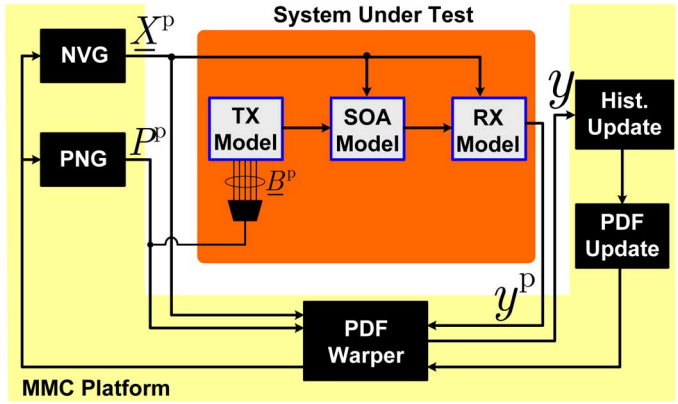

Fig. 8. Block diagram of the simulator; NVG: random vector generator, PNG: pattern number generator.

r_0. The vector of all noise samples is denoted by $\underline{X}$, which is explicitly written as

$$\underline{X} \triangleq [\tilde{n}_{ASE}^{SOA}, \tilde{n}_{ASE}^{Rec}, n_R] \tag{25}$$

where $\tilde{n}_{ASE}^{SOA}$ and $\tilde{n}_{ASE}^{Rec}$ are vectors of independent identically distributed white complex Gaussian noise samples each of length MN_s; the former accounts for ASE noise from the SOA (cf. Fig. 2), and the latter accounts the ASE of the pre-amplified receiver (cf. Fig. 7); n_R is a real Gaussian random variable with proper mean and variance modeling the receiver noise (cf. Fig. 7). The vector $\underline{B}$ contains all the past bits falling in the effective memory of the link

$$\underline{B} \triangleq [b_{-1}, \ldots, b_{-M}] \tag{26}$$

The noise vector generator (NVG) subsystems in Fig. 8 is a Metropolis-Hastings machine [31], which proposes noise vector samples $\underline{X}^{\mathrm{p}}$. The pattern number generator (PNG) subsystem in Fig. 8 is an other Metropolis-Hastings machine, proposing pattern numbers P^{p}; the binary representation of a pattern number is the bit pattern. The PDF warper accepts or rejects the proposals from NVG and PNG $[\underline{X}^{\mathrm{p}}; P^{\mathrm{p}}]$ according to the MMC algorithm. Consequently, the PNG performs a random walk over the index in the summation of (24), while the NVG performs a random walk to explore the conditional PDFs within the sum.

IV. Experimental Results

The experimental setup is shown in Fig. 9. We performed two different measurements: RX1 to directly measure the conditional PDFs of marks and spaces, and RX2 to measure the BER.

A. Conditional PDFs

We developed an experimental technique, new to our knowledge, to directly measure the conditional PDFs of marks and spaces using a PC-controlled 50 GHz Agilent 86116A sampling scope. We must unambiguously determine the samples corresponding to marks and spaces at the receiver; then the histogram can be computed. To this end we transmit many packets

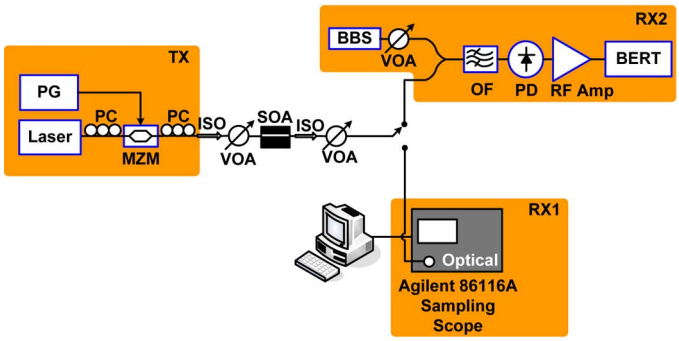

Fig. 9. Experimental setup to measure conditional PDFs (RX1) and BER (RX2); PG: pattern generator, MZM: Mach–Zehnder modulator, PC: polarization controller, VOA: variable optical attenuator, ISO: isolator, OF: optical filter, PD: photodetector, BERT: BER tester.

consisting of a De Bruijn sequence preceded by a header of N_1 marks followed by N_0 spaces. The DeBruijn sequence of length 2^m is obtained by appending a zero to the end of a PRBS sequence of length $2^m - 1$. All possible m-bit patterns appear exactly once in a DeBruijn sequence of length 2^m, such that, if it is used as the transmitted pattern, all summands in (24) are visited with equal frequency. Processing consists of filtering the zero-averaged packet by a moving average filter of length N_1 and detecting the peak. The location of the peak coincides with the one-to-zero transition in the header; once the header is synchronized, the transmitted sequence can be identified without error. The principles of this technique are illustrated in Fig. 10(a).

Several practical considerations enter into setting various parameters. The sequence length $2^{M_{seq}}$ should have M_{seq} bigger than the (unknown) effective memory of the link. De Bruijn sequences end with a series of zeros; to distinguish the one-to-zero transition in the header we require $N_1 > M_{seq}$. Increasing N_1 results in more pronounced peaks in the filtered zero-averaged packet; if the OSNR is low, the conditional PDFs of marks and spaces overlap considerably, and we must use a large N_1.

Finally, the temporal setting of the scope, the bit-rate, and the packet length should satisfy two necessary conditions for the measurements to be stable. Suppose the buffer length of the scope is denoted by N_w (for the Agilent 86116A the maximum is 4096). If we want N_s samples per bit, the sampling time is $dt = T_b/N_s$, and the temporal width of the scope's buffer is $T_w = N_w dt$; on the other hand, if the time per division of scope is ΔT, we have $T_w = 10\Delta T$. Therefore the following condition should hold

$$\frac{N_w}{N_s} = \frac{10\Delta T}{T_b}. \tag{27}$$

Clearly the packet must fit in the buffer so

$$N_w \geqslant N_1 + N_0 + 2^{M_{seq}} \tag{28}$$

We do not know the length of the SOA effective memory *a priori*; but we can sound the memory depth of SOA as is depicted in Fig. 10(b). We measured the conditional PDFs

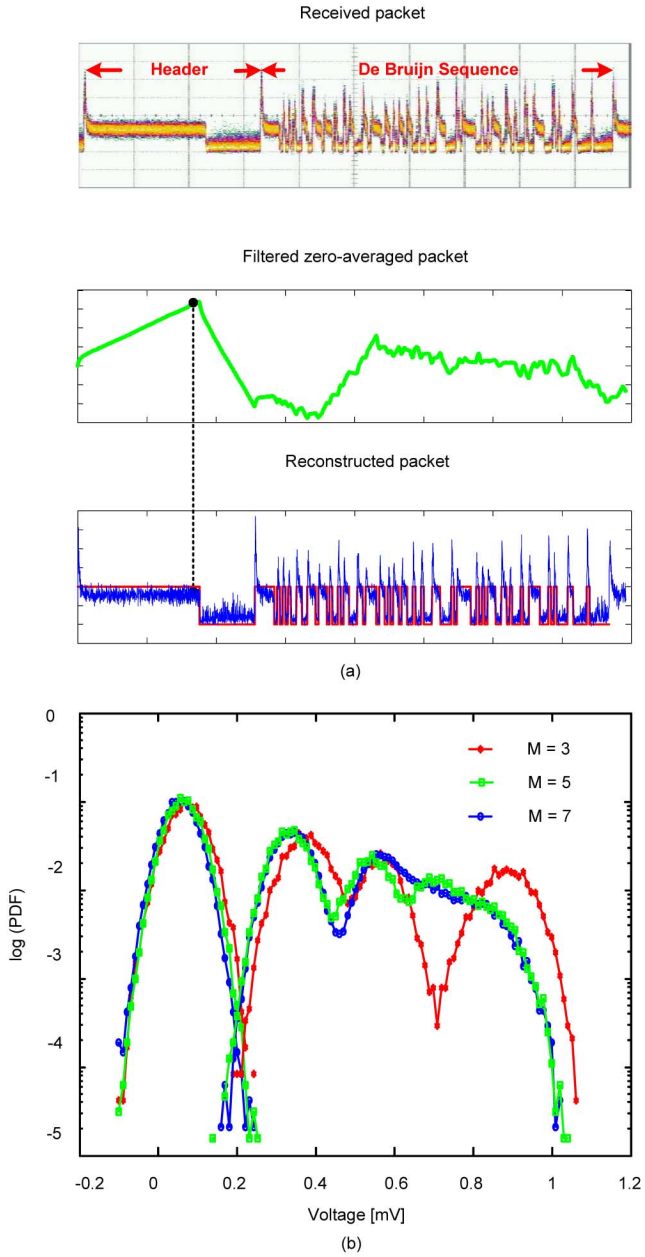

Fig. 10. (a) Steps to measure the conditional PDF using the packetized De Bruijn sequence; (b) conditional PDFs of marks and spaces measured for three different length De Bruijn sequences in the packet payload.

for various lengths of the De Bruijn sequence: $M_{seq} = 3$, 5, 7. When M_{seq} is smaller than the link effective memory, the measured PDFs are meaningless; as M_{seq} approaches the effective memory, the measured conditional PDFs approach the true PDFs. Note that the memory sounding can also be done in software by estimating the truncated conditional PDFs for increasing values of M.

Fig. 11 illustrates measured and simulated conditional PDFs of marks and spaces when $M_{seq} = 7$. The SOA input power was -2.65 dBm, resulting in deep saturation; the bit-rate was 10 Gb/s. The PDFs were calculated at the middle of the bit. Simulation results are for five MMC cycles of 10^5 samples each;

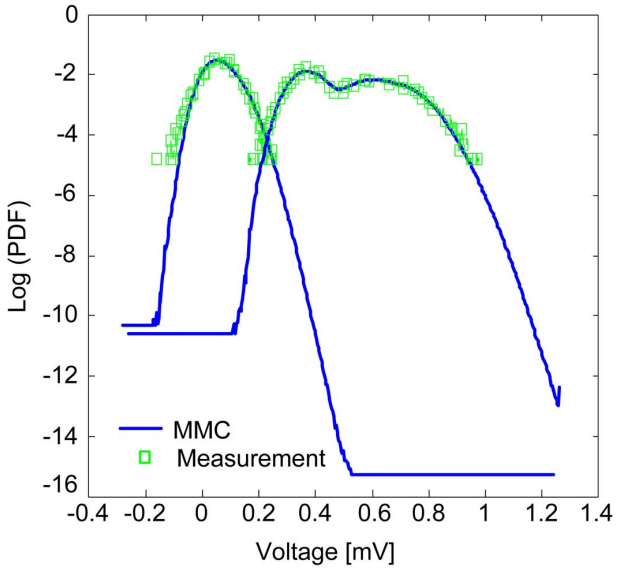

Fig. 11. Measured and simulated conditional PDFs of marks and spaces.

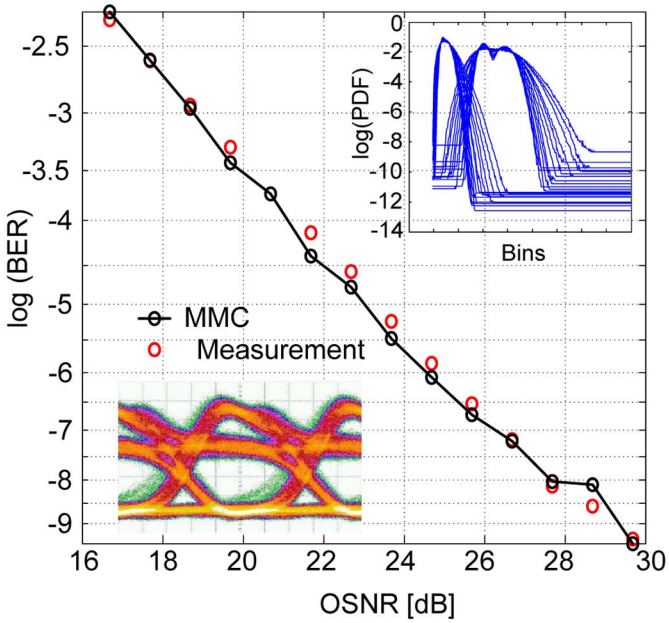

Fig. 12. Measured and simulated BERs at RX2; upper inset shows the conditional PDFs used to estimate the BER curve (one pair per BER curve point), lower inset is eye diagram for lowest BER estimated.

each cycle took 71 seconds to execute. In Fig. 11, only the PDFs corresponding to the last cycle are shown.

Using RX2, we measured the BER as a function of the received OSNR and present these results in Fig. 12. The SOA average input power and the bit-rate were set as in the previous case. MMC simulations (one for conditional PDF of marks, the other for spaces) were required at each BER point; the BER was computed by numerically integrating the overlapping tails of estimated conditional PDFs of marks and spaces. Each PDF estimation included seven MMC iterations, to improve the accuracy. In the lower inset of Fig. 12 we show an eye diagram for high OSNR that clearly depicts the strong patterning effect from the SOA. The upper inset is the set of estimated conditional PDFs used to calculate one BER point.

V. Conclusion

We presented a new simulation tool based on MMC to accurately model an optical link containing a nonlinear SOA. We verified experimentally that our simulator can accurately characterize the received signal statistics in the presence of high bit patterning due to the saturated SOA. We introduced an experimental technique to directly measure the conditional PDFs using a sampling scope, experimentally probed the effective memory of SOA, and were able to accurately predict the measured PDFs and BER with our simulator. The purely numerical nature of the simulator allows for the exact nonlinear dynamics of the SOA to be captured, and the use of MMC makes it fast and efficient. Besides being a design and optimization tool per se, it can be used to 1) examine the accuracy of analytical approximations, 2) reduce computation time, and 3) study the impact of changing the modulation format on performance. Moreover, by adding features to the SOA model of (19), the impact of ultrafast processes, nonlinear polarization rotation, enhanced phase dynamics, and interchannel effects in the multichannel regime can in principle be assessed.

References

[1] T. Durhuus, B. Mikkelsen, C. Joergensen, S. L. Danielsen, and K. E. Stubkjaer, "All-optical wavelength conversion by semiconductor," *J. Lightw. Technol.*, vol. 14, pp. 942–954, 1996.

[2] O. Leclerc, B. Lavigne, E. Balmefrezol, P. Brindel, L. Pierre, D. Rouvillain, and F. Seguineau, "Optical regeneration at 40 Gb/s and beyond," *J. Lightw. Technol.*, vol. 21, pp. 2779–2790, 2003.

[3] Z. Zhu, M. Funabashi, Z. Pan, B. Xiang, L. Paraschis, and S. J. B. Yoo, "Jitter and amplitude noise accumulations in cascaded all-optical regenerators," *J. Lightw. Technol.*, vol. 26, pp. 1640–1652, 2008.

[4] A. D. McCoy, P. Horak, B. C. Thomsen, M. Ibsen, and D. J. Richardson, "Noise suppression of incoherent light using a gain-saturated SOA: Implications for spectrum-sliced WDM systems," *J. Lightw. Technol.*, vol. 23, pp. 2399–2409, 2005.

[5] J. D. Downie, J. Hurley, and Y. Mauro, "10.7 Gb/s uncompensated transmission over a 470 km hybrid fiber link with in-line SOAs using MLSE and duobinary signals," *Optics Express*, vol. 16, pp. 15759–15764, 2008.

[6] E. Forestieri, "Evaluating the error probability in lightwave systems with chromatic dispersion, arbitrary pulse shape and pre-and postdetection filtering," *J. Lightw. Technol.*, vol. 18, pp. 1493–1503, 2000.

[7] P. Serena, A. Orlandini, and A. Bononi, "Parametric-gain approach to the analysis of single-channel DPSK/DQPSK systems with nonlinear phase noise," *J. Lightw. Technol.*, vol. 24, pp. 2026–2037, 2006.

[8] M. C. Jeruchim, "Techniques for estimating the bit error rate in the simulation of digital communication systems," *J. Sel. Areas Commun.*, vol. SAC-2, pp. 153–170, 1984.

[9] M. J. Connelly, *Semiconductor Optical Amplifiers*. New York: Springer-Verlag, 2002.

[10] G. P. Agrawal and N. A. Olsson, "Self-phase modulation and spectral broadening of optical pulses in semiconductor laser amplifiers," *IEEE J. Quantum Electron.*, vol. 25, pp. 2297–2306, 1989.

[11] D. Cassioli, S. Scotti, and A. Mecozzi, "A time-domain computer simulator of the nonlinear response of semiconductor optical amplifiers," *IEEE J. Quantum Electron.*, vol. 36, no. 7, pp. 1072–1080, 2000.

[12] M. J. Connelly, "Wide-band steady-state numerical model and parameter extraction of a tensile-strained bulk semiconductor optical amplifier," *IEEE J. Quantum Electron.*, vol. 43, pp. 47–56, 2007.

[13] A. Bogoni, L. Poti, C. Porzi, M. Scaffardi, P. Ghelfi, and F. Ponzini, "Modeling and measurement of noisy SOA dynamics for ultrafast applications," *IEEE Sel. Topics Quantum Electron.*, vol. 10, pp. 197–205, 2004.

[14] L. Occhi, L. Schares, and G. Guekos, "Phase modeling based on the α-factor in bulk semiconductor optical amplifiers," *IEEE Sel. Topics Quantum Electron.*, vol. 9, pp. 788–797, 2003.

[15] H. J. S. Dorren, D. Lenstra, L. Yong, M. T. Hill, and G.-D. Khoe, "Nonlinear polarization rotation in semiconductor optical amplifiers: Theory and application to all-optical flip-flop memories," *IEEE J. Quantum Electron.*, vol. 39, pp. 141–148, 2003.
[16] F. Ohman, J. Mork, and B. Tromborg, "Output power PDF of a saturated semiconductor optical amplifier: Second-order noise contributions by path integral method," *IEEE J. Quantum Electron.*, vol. 43, pp. 1188–1197, 2007.
[17] A. A. M. Saleh and I. M. I. Habbab, "Effects of semiconductor-optical-amplifier nonlinearity on the performance of high-speed intensity-modulation lightwave systems," *IEEE Trans. Commun.*, vol. 38, pp. 839–846, 1990.
[18] A. Bilenca and G. Eisenstein, "Statistical noise properties of an optical pulse propagating in a nonlinear semiconductor optical amplifier," *IEEE J. Quantum Electron.*, vol. 41, pp. 36–44, 2005.
[19] A. Bilenca and G. Eisenstein, "Fokker-Planck and Langevin analyses of noise accompanying the amplification of optical pulses in semiconductor optical amplifiers," *J. Opt. Soc. Am. B*, vol. 22, pp. 1632–1639, 2005.
[20] A. Ghazisaeidi, F. Vacondio, A. Bononi, and L. A. Rusch, "SOA intensity noise suppression in spectrum sliced systems: A multicanonical Monte Carlo simulator of extremely low BER," *J. Lightw. Technol.*, vol. 27, no. 14, pp. 2667–2677, Jul. 2009.
[21] L. Gerardi, M. Secondini, and E. Forestieri, "Pattern perturbation method for multicanonical Monte Carlo simulations in optical communications," *IEEE Photon. Technol. Lett.*, vol. 19, no. 23, pp. 1934–1936, 2007.
[22] A. Ghazisaeidi, F. Vacondio, A. Bononi, and L. A. Rusch, "Statistical characterization of bit patterning in SOAs: BER prediction and experimental validation," in *OFC2009*, OWE7.
[23] A. A. M. Saleh, "Nonlinear models of traveling-wave optical amplifiers," *Electron. Lett.*, vol. 24, no. 14, pp. 835–837, 1988.
[24] A. Bononi and L. Barbieri, "Design of gain-clamped doped-fiber amplifiers for optimal dynamic performance," *J. Lightw. Technol.*, vol. 17, pp. 1229–1240, 1999.
[25] X. Wei and L. Zhang, "Analysis of the phase noise in saturated SOAs for DPSK applications," *IEEE J. Quantum Electron.*, vol. 41, pp. 554–561, 2005.
[26] F. S. Hill, Jr. and M. A. Blanco, "Random geometric series and intersymbol interference," *IEEE Trans. Inf. Theory*, vol. IT-19, pp. 326–335, 1973.
[27] M. L. Nielsen, J. Mørk, R. Suzuki, J. Sakaguchi, and Y. Ueno, "Experimental and theoretical investigation of the impact of ultra-fast carrier dynamics on high-speed SOA-based all-optical switches," *Optics Express*, vol. 14, pp. 331–347, 2006.
[28] T. Akiyama, M. Sugawara, and Y. Arakawa, "Quantum-dot semiconductor optical amplifiers," *Proc. IEEE*, vol. 95, no. 9, pp. 1757–1766, 2007.
[29] I. Kang, C. Dorrer, L. Zhang, M. Dinu, M. Rasras, L. L. Buhl, S. Cabot, A. Bhardwaj, X. Liu, M. A. Cappuzzo, L. Gomez, A. Wong-Foy, Y. F. Chen, N. K. Dutta, S. S. Patel, D. T. Neilson, C. R. Giles, A. Piccirilli, and J. Jaques, "Characterization of the dynamical processes in all-optical signal processing using semiconductor optical amplifiers," *IEEE J. Sel. Topics Quantum Electron.*, vol. 14, no. 3, pp. 758–769, 2008.
[30] G. P. Agrawal, *Applications of Nonlinear Fiber Optics*. Boston, MA: Academic Press, 2001, pp. 138–141.
[31] D. J. C. MacKay, *Information Theory, Inference, and Learning Algorithms*.. Cambridge, U.K.: Cambridge Univ. Press, 2003, pp. 357–387.

Amirhossein Ghazisaeidi received the M.A. degree in communications systems and the B.S. degree in electrical engineering from Sharif University of Technology, Tehran, Iran. He is currently working toward the Ph.D. in the Department of Electrical and Computer Engineering, Laval University, Quebec, Canada.

His research interests include optical-code-division multiple access and spectrum sliced WDM using incoherent sources, dynamics, and noise properties of optical amplifiers, modeling optoelectronic devices, and performance analysis of optical links.

Francesco Vacondio was born in Reggio Emilia, Italy, in 1981. In October 2006 he received the "Laurea Magistrale" degree (*cum laude*) in telecommunications engineering from the University of Parma, Parma, Italy. Since September 2005 he has also been with the Department of Electrical and Computer Engineering at Laval University, Quebec, Canada, where his research interests include semiconductor optical amplifiers, phase modulated formats and microwave photonics.

Alberto Bononi (M'09) received the Laurea degree in electronics engineering (*cum laude*) from the University of Pisa, Pisa, Italy, in 1988, and the M.A. and Ph.D. degrees in electrical engineering from Princeton University, Princeton, NJ, in 1992 and 1994, respectively.

Currently, he is an Associate Professor of Telecommunications at the School of Engineering, Università di Parma, Italy. He teaches courses in Probability Theory and Stochastic Processes, Telecommunications Networks, and Optical Communications. In 1990, he worked at GEC-Marconi Hirst Research Centre, Wembley, U.K., on a Marconi S.p.A. project on coherent optical systems. From 1994 to 1996, he was an Assistant Professor in the Electrical and Computer Engineering Department at the State University of New York (SUNY), Buffalo, teaching courses in Electric Circuits and Optical Networks. In the summers of 1997 and 1999, he was a Visiting Faculty at the Département de Genie Électrique, Université Laval, QC, Canada, doing research on fiber amplifiers. His present research interests include system design and performance analysis of high-speed all-optical networks, nonlinear fiber transmission for WDM systems, linear and nonlinear polarization mode dispersion, and transient gain dynamics in optical amplifiers.

Leslie Ann Rusch (S'91–M'94–SM'00–F'10) received the B.S.E.E. (honors) degree from the California Institute of Technology, Pasadena, in 1980 and the M.A. and Ph.D. degrees in electrical engineering from Princeton University, Princeton, NJ, in 1992 and 1994, respectively.

In 1994 she joined the Department of Electrical and Computer Engineering at Laval University, Quebec, Canada, where she is currently a Full Professor performing research in wireless and optical communications. She spent two years as the manager of a group researching new wireless technologies at Intel Corporation from 2001 to 2002. Her research interests include optical-code-division multiple access and spectrum sliced WDM using incoherent sources for passive optical networks; semiconductor and erbium-doped optical amplifiers and their dynamics; radio over fiber; and in wireless communications, high performance, reduced complexity receivers for ultra-wide-band systems employing optical processing.